AIAA JOURNAL
Vol. 32, No. 5, May 1994

Grid Adaptation Using Chimera Composite Overlapping Meshes

Kai-Hsiung Kao* and Meng-Sing Liou†
NASA Lewis Research Center, Cleveland, Ohio 44135
and
Chuen-Yen Chow‡
University of Colorado, Boulder, Colorado 80309

The objective of this paper is to perform grid adaptation using composite overlapping meshes in regions of large gradient to accurately capture the salient features during computation. The chimera grid scheme, a multiple overset mesh technique, is used in combination with a Navier-Stokes solver. The numerical solution is first converged to a steady state based on an initial coarse mesh. Solution-adaptive enhancement is then performed by using a secondary fine grid system which oversets on top of the base grid in the high-gradient region, but without requiring the mesh boundaries to join in any special way. Communications through boundary interfaces between those separated grids are carried out using trilinear interpolation. Applications to the Euler equations for shock reflections and to a shock wave/boundary layer interaction problem are tested. With the present method, the salient features are well-resolved.

I. Introduction

DURING the last decade both structured and unstructured grid systems have been developed and applied for computations in various computational fluid dynamics problems. It is well-known that the accuracy of the computational solutions to analytical equations is strongly influenced by the discretization of the space in which a solution is sought. In general, the introduction of a highly dense distribution of points throughout a computational domain will yield a more accurate answer than a coarse distribution. However, limitations in computer processing speed and accessible memory prohibit such a scenario. An appropriate alternative, for example a grid adaptation method, would be to improve the accuracy of the computation where needed.

Many different solution-adaptive techniques have been developed and implemented. Gnoffo[2] modeled the mesh as a network of springs whose constants were determined from flowfield gradients. Brackbill[3] and Saltzman and Brackbill[4] used variational methods. Berger[5] developed an adaptive refinement method which dynamically embedded finer and finer grids to resolve flow gradients. Eiseman[6,7] developed the method of mean value relaxation and reviewed existing adaptation concepts. Other adaptive methods are based upon equidistribution techniques; Nakahashi and Deiwert[8] used a spring-torsion analogy to adapt the grid, while Gonnett et al.[9,10] based their algorithm on the method of minimal moments. The idea of a patched mesh technique has been applied by Lombard and Venkatapathy[11] and Venkatapathy and Lombard[12] to capture sharp shock structures. Recently, computational investigation of vortical flows over a delta wing was carried out by Ekaterinaris and Schiff[13] using the zonal grid approach.

Many works have been devoted to developing techniques and methods that address two major problem areas in grid generation. They are: 1) the large amount of time required to generate a grid for a complex domain, and 2) the ability to generate a grid that meets the users quality requirements (e.g., smoothness, clustering, orthogonality). Unfortunately, grid adaptation techniques usually create high-aspect-ratio or highly skewed cells to align with the high-gradient features, resulting in a reduced convergence history.

A general motivation of the present study is to develop a grid adaptation method that not only enhances the accuracy of solutions by using a fine grid in high-gradient regions, but one that is also capable of handling complex geometries with cells of minimal skewedness. The present methodology uses the chimera composite overlapping mesh system[1] to improve geometric flexibility and to achieve grid adaptation efficiently. It is proposed that composite grid schemes use two or more simple meshes to capture the salient features in complex flows. The use of a multiple grid approach can yield better grid resolution, simplify the application of boundary conditions, and ease the task of grid generation. Because the overset meshes are independent of each other and the global mesh, they can readily be embedded in arbitrary orientations with respect to the global grid. This approach has the following two merits. First, it gives geometrical independence in the process of grid generation. Second, it allows natural alignment and clustering of grid points to enhance the accuracy of the flow solution.

In the following sections, we describe the governing equations, the flow solver algorithm, and the solution-adaptive enhancement method using chimera overlapping meshes. Applications are presented for shock reflection, 15-deg ramp channel, flat-plate boundary layer and shock wave/boundary layer interaction problems.

II. Governing Equations

The Navier-Stokes equations can be expressed in an integral form in a volume v with enclosing surface s as follows:

$$\int_v \frac{\partial U}{\partial t}\,dv + \oint_s \boldsymbol{n}\,ds \cdot (F - F_v) = 0 \tag{1}$$

where the conservative variable U is

$$U = [\rho, \rho \boldsymbol{u}, \rho E]^T$$

the inviscid flux F is

$$F = [\rho \boldsymbol{u}, \rho \boldsymbol{u}\boldsymbol{u} + p\tilde{I}, \rho H \boldsymbol{u}]^T$$

the viscous flux F_v is

$$F_v = [0, \tilde{\tau}, \tilde{\tau}\boldsymbol{u} + \boldsymbol{q}]^T$$

Received March 13, 1993; presented as Paper 93-3389 at the AIAA 11th Computational Fluid Dynamics Conference, Orlando, FL, July 6–9, 1993; revision received Aug. 31, 1993; accepted for publication Sept. 2, 1993. This paper is declared a work of the U.S. Government and is not subject to copyright protection in the United States.

*Senior Research Associate, Institute for Computational Mechanics in Propulsion. Member AIAA.
†Senior Research Scientist. Member AIAA.
‡Professor, Department of Aerospace Engineering Sciences. Associate Fellow AIAA.

and the equation of state for ideal gas is

$$p = (\gamma - 1)\rho e \tag{2}$$

Here e represents the internal energy. The vector quantities, expressed in terms of Cartesian coordinates, are denoted with boldface type, and the tensor with an overhead tilde (~) or a dyadic notation such as $\boldsymbol{uu}$.

Assuming a Newtonian fluid and using Stoke's hypothesis, the stress tensor $\tilde{\tau}$ and the heat flux vector $\tilde{q}$ are expressed in terms of the gradient (∇) of relevant quantities:

$$\tilde{\tau} = -\frac{2}{3}\mu_v(\nabla\cdot\boldsymbol{u})\tilde{I} + \mu_v[\nabla\boldsymbol{u} + (\nabla\boldsymbol{u})^T]$$

$$\boldsymbol{q} = \mu_e \nabla e$$

The transport coefficients for the momentum and heat fluxes are μ_v and μ_e, respectively. In this paper, we restrict our study to laminar flows only. The laminar viscosity is given by the Sutherland law and the Prandtl number is assumed to be constant at 0.72 throughout the flowfields.

III. Numerical Methods

Chimera Grid Scheme

The chimera scheme is a grid embedding technique which provides a conceptually simple method for domain decomposition. For instance, a major grid is usually generated about a main body element and minor grids are then overset on the major grid so as to resolve interesting features of the configuration. Usually, the minor grids are overset on top of the major grid without requiring the mesh boundaries to join in any special way. However, a common or overlap region is always required to provide a means of matching the solutions across boundary interfaces.

To increase the flexibility in the selection of subdomains, the chimera scheme also allows an implementation to remove regions of a mesh containing an embedded grid from that mesh. That is, an embedded mesh introduces a "hole" into the mesh in which it is embedded. Typically, a hole is defined by a creation boundary which consists of a surface or a group of surfaces. The purpose of a hole creation boundary is to identify points that are within this boundary. A mesh point is considered to be inside a hole creation boundary if it is inside all surfaces that define the boundary. Figure 1 illustrates the method used to determine whether a point is inside or outside a surface. A mesh point P is considered to be inside a surface if the dot product between $\boldsymbol{R}$ (the vector from the closest point on the surface to the mesh point), and $\boldsymbol{N}$ (the normal vector

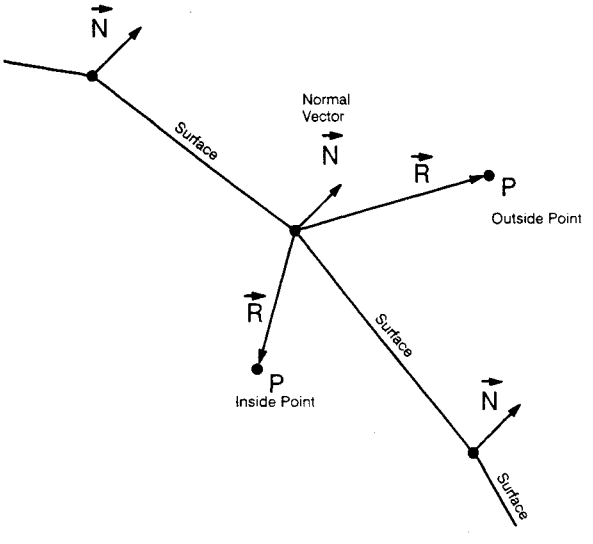

Fig. 1 Mesh point considered to be inside or outside of surface.[14]

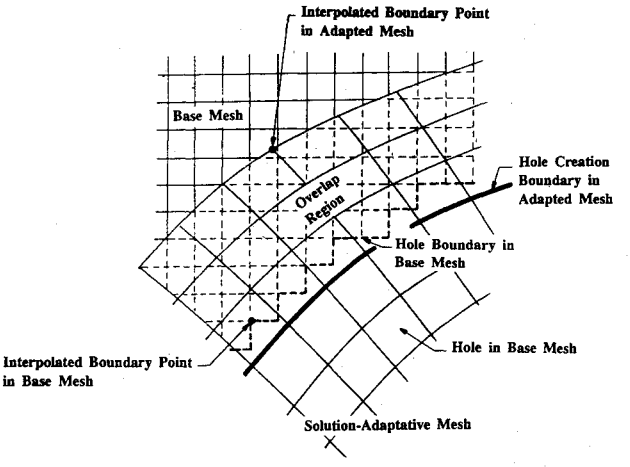

Fig. 2 Overset grids for base mesh and solution-adaptive mesh.[14]

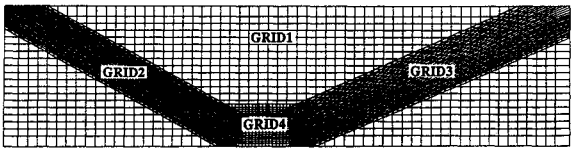

Fig. 3 Composite overlapping grid system for inviscid shock reflection problem; GRID1 (59 × 20), GRID2 (29 × 50), GRID3 (29 × 50), and GRID4 (29 × 20).

on the surface at the closest point, directed outward from the hole region) is negative or zero. If the dot product is positive, the mesh point is considered to be outside the surface. Because the regions interior to the hole do not enter into the solution process, intergrid communication is simplified since communication among the grids is restricted to the transfer of boundary data. Appropriate boundary values are interpolated from the mesh or meshes in which the boundary is embedded. Communication between overlaid grids is achieved by interpolation of boundary values from grids in which the boundaries are contained. The scheme employs nonconservative, trilinear interpolation that, as some simple experiments have shown, is superior to Taylor series expansion. The question of conservative vs nonconservative interpolation is beyond the scope of the present study, and will be a topic of future investigations.

The chimera procedure naturally separates into two parts: generation of the composite mesh and associated interpolation data and solution of the flow model. The first part has been embodied in a computer code, PEGSUS.[14] PEGSUS takes the independently generated component grids and the embedding structure as input and automatically constructs the composite mesh and interpolation data which are output. More details regarding the embedding grid technique can be found in Ref. 15.

Flow Solver

A computer code based on a time-accurate, three-dimensional, finite-volume, high-resolution scheme for solving the compressible, full Navier-Stokes equations has been developed.[16] Based on the finite-volume method, Eq. (1) is semidiscretized by assuming that the cell-centered conserved variables are constant within a cell, and that the flux integral at cell surfaces is also approximated by an average value of the numerical flux. The numerical formulation uses a new class of flux splitting schemes.[17,18] The scheme first splits the full flux into convective and pressure fluxes, $F_{1/2}^{(c)}$ and $F_{1/2}^{(p)}$, respectively,

$$F_{1/2} = F_{1/2}^{(c)} + F_{1/2}^{(p)} = c_{1/2}\Phi_{L/R} + P_{1/2} \tag{3}$$

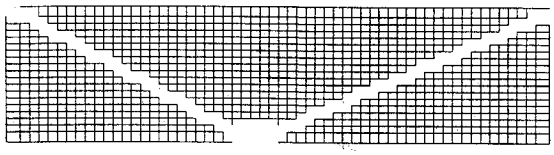

Fig. 4 Background mesh (GRID1) with "hole" grids blanked in high-gradient regions.

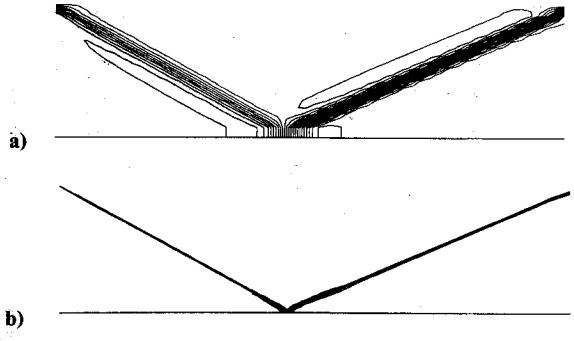

Fig. 5 Pressure contours for shock reflection problem: a) single grid 59 × 20 and b) overlapping grids (M_∞ = 2.9, shock angle = 29 deg, p_{min} = 0.6, p_{max} = 4.0, Δp = 0.1).

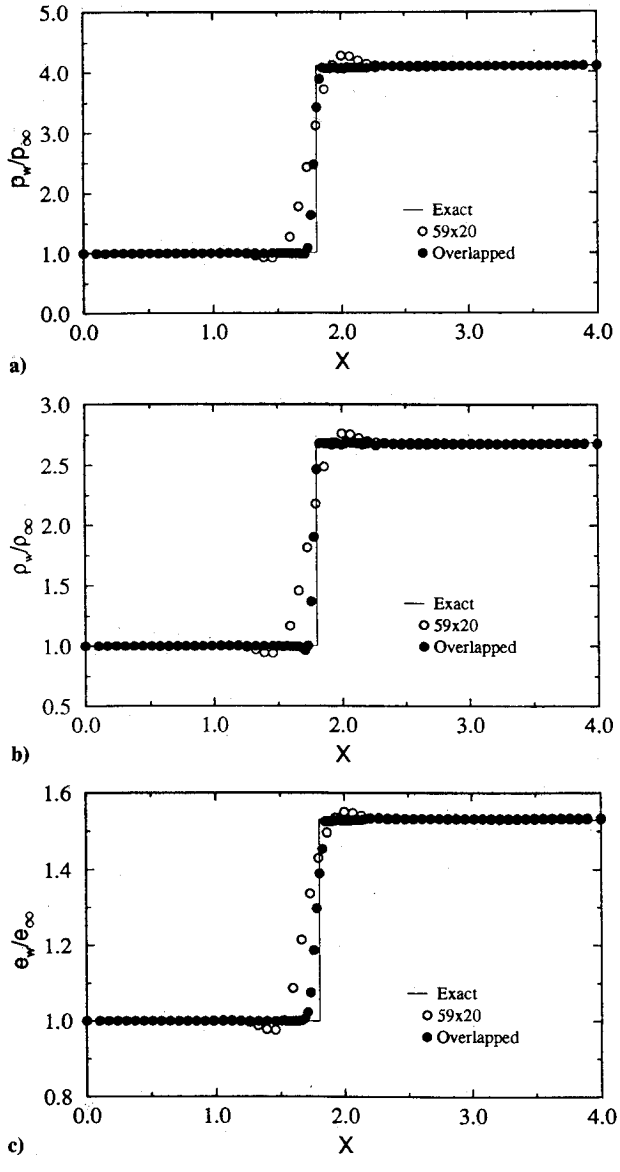

Fig. 6 Variable profiles along solid surface (y = 0) for inviscid shock reflection problem: a) pressure, b) density, and c) internal energy.

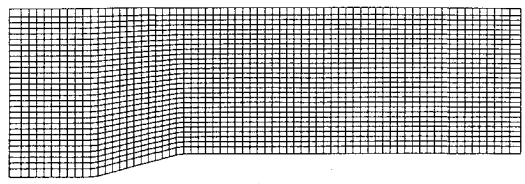

Fig. 7a Single coarse grid (69 × 30) for a 15-deg ramp channel flow.

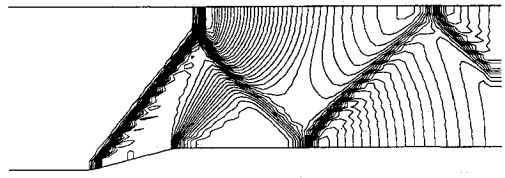

Fig. 7b Pressure contours for a 15-deg ramp channel flow (69 × 30), (M_∞ = 1.8, p_{min} = 0.7, p_{max} = 2.7, Δp = 0.05).

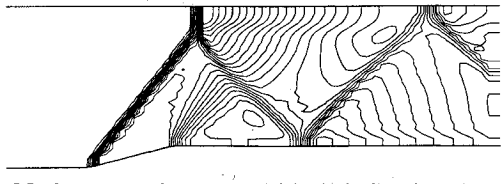

Fig. 7c Mach contours for a M_∞ = 1.8 inviscid flow in a channel with a 15-deg ramp (M_{min} = 0.6, M_{max} = 1.8, ΔM = 0.05, 69 × 30).

at the cell interface $L < 1/2 < R$. The interface pressure $P_{1/2}$ simply comprises the "positive" and "negative" data from appropriate domains of dependence via characteristic speed decomposition. The passive scalar variables $\Phi \equiv (\rho, \rho u, \rho H)^T$ are transported by a common convective velocity $u_{1/2}$ that is constructed in a similar fashion as $P_{1/2}$. Then the upwind idea is used to select the state, i.e., L or R, of the variables to be convected. As such, the interface flux can be recast in the following form:

$$F_{1/2} = c_{1/2}\, 1/2\,[\Phi_L + \Phi_R] - 1/2|c_{1/2}|\Delta_{1/2}\Phi + P_{1/2} \tag{4}$$

where $\Delta_{1/2}( ) = ( )_R - ( )_L$. Here the first term on the right-hand side is clearly not a simple average of the L and R fluxes, but rather a weighted average via the convective velocity.

A variant of the second-order, time-accurate, Lax-Wendroff method is proposed that utilizes identical procedures in both predictor and corrector steps:

$$\text{predictor:} \quad U^* = U^n + \Delta t \frac{\partial U^n}{\partial t}$$

$$\text{corrector:} \quad U^{**} = U^* + \Delta t \frac{\partial U^*}{\partial t} \tag{5}$$

$$U^{n+1} = 1/2\,(U^n + U^{**})$$

As mentioned before, a flow solver must be modified to account for the use of multiple meshes and the holes in the grids. These hole points must be blanked or excluded from the flowfield solution. The main change in the flow algorithm itself is the treatment of the hole boundaries. The PEGSUS code is used to determine the interpolation coefficients between composite grids. The hole information from the chimera grid package is stored in an array, IBLANK, which is defined for each point on each grid as

$$\text{IBLANK} = \begin{cases} 1, & \text{if a point is not blanked} \\ 0, & \text{if a point is blanked} \end{cases}$$

In the flow solver, each element in the corrector step is multiplied by the appropriate IBLANK value before the solutions are updated:

$$U^{n+1} = U^n + \text{IBLANK} \cdot (U^{n+1} - U^n) \tag{6}$$

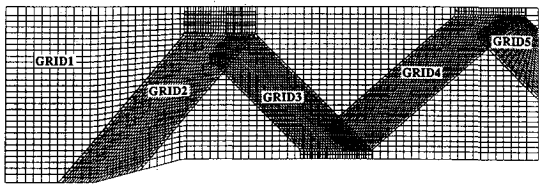

Fig. 8a Composite overlapping grid system for a 15-deg ramp channel flow; GRID1 (69 × 30), GRID2 (29 × 50), GRID3 (29 × 50), GRID4 (29 × 50), and GRID5 (29 × 20).

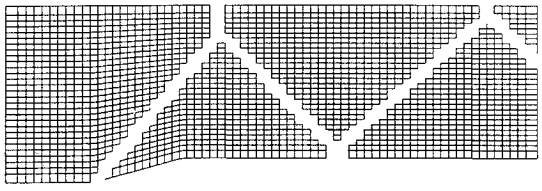

Fig. 8b Base grid (GRID1) with "hole" grids blanked in high-gradient regions.

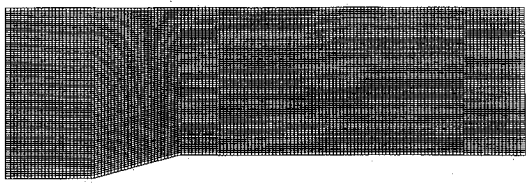

Fig. 9a Fine grid mesh (149 × 80) for a 15-deg ramp channel flow.

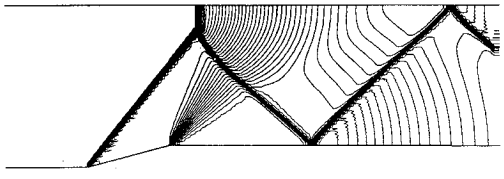

Fig. 9b Pressure contours for a 15-deg ramp channel flow, 149 × 80 ($M_\infty = 1.8$, $p_{min} = 0.7$, $p_{max} = 2.7$, $\Delta p = 0.05$).

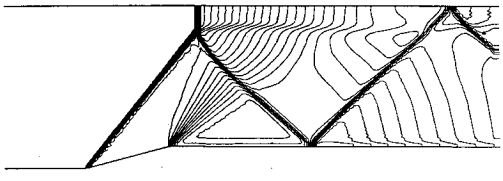

Fig. 9c Mach contours for a $M_\infty = 1.8$ inviscid flow in a channel with a 15-deg ramp ($M_{min} = 0.6$, $M_{max} = 1.8$, $\Delta M = 0.05$, 149 × 80).

The blanked solutions are updated in the interpolation routine. With this approach, no special routines or logic tests are required to exclude the blanked points from the flowfield solution.

Solution-Adaptive Overlaid Meshes

It is proposed that the chimera overset grids be applied to enhance the solution by adapting additional grid meshes over salient flow features. We first obtain a sufficiently converged solution based on a reasonably coarse grid and then adapt a secondary grid mesh which is clustered and aligned with the solution features such as a shock wave, contact surface, boundary layer, and shear layer. In the shock wave problem, we adapt a fine-mesh system to the shock location without requiring the mesh boundaries to join in any special way. Subsequently, grid points within those high-gradient regions are blanked or excluded from the base grid—i.e., a hole is created on the base (coarse) grid. Communications through boundary interfaces between those separate grids are carried out using trilinear interpolation. Figure 2 illustrates the connections between composite overlapping grids, with hole points being blanked by a prescribed flow feature such as the shock wave.

To be specific, the present methodology applies additional structured overset grid meshes to align and/or cluster with the salient features in the flowfield. In this case, no grid points will be sacrificed in the base (coarse) mesh so that the overall accuracy of

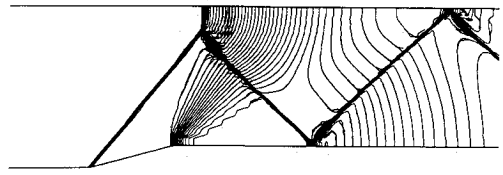

Fig. 8c Pressure contours for a 15-deg ramp channel flow with composite adaptive meshes ($M_\infty = 1.8$, $p_{min} = 0.7$, $p_{max} = 2.7$, $\Delta p = 0.05$).

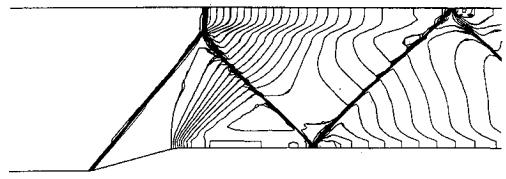

Fig. 8d Mach contours for a $M_\infty = 1.8$ inviscid flow in a channel with a 15-deg ramp ($M_{min} = 0.6$, $M_{max} = 1.8$, $\Delta M = 0.05$, adapted overlapping meshes).

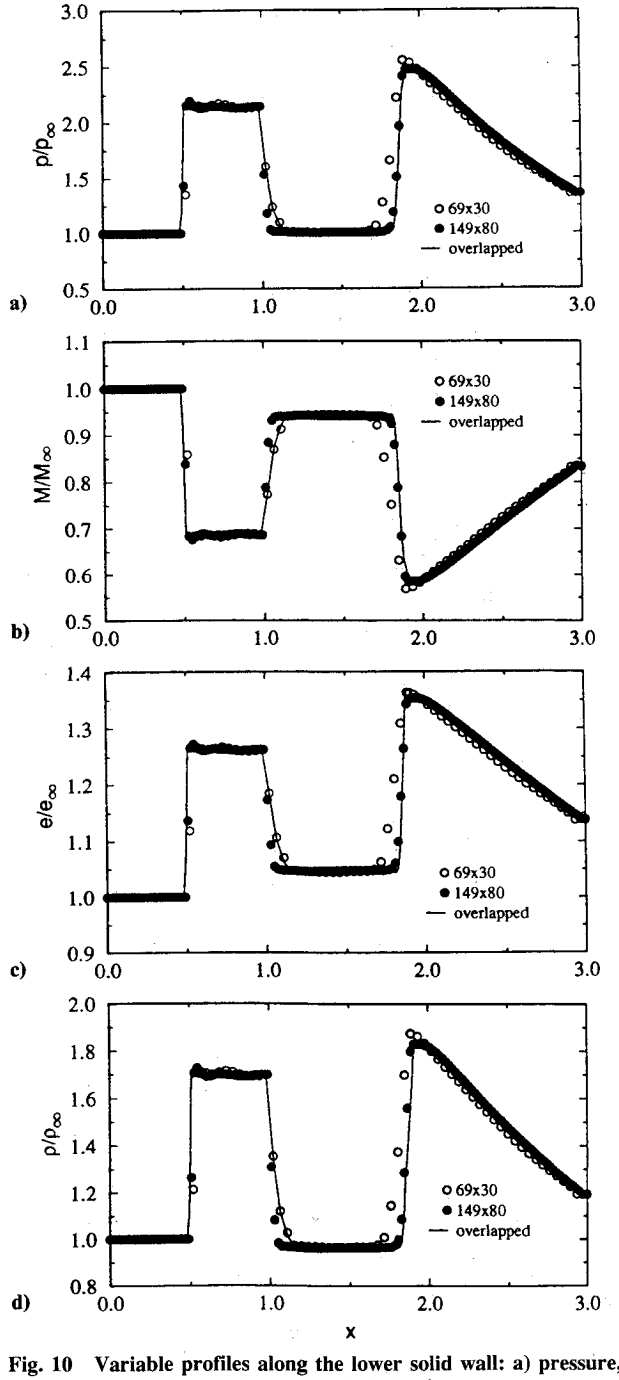

Fig. 10 Variable profiles along the lower solid wall: a) pressure, b) Mach number, c) internal energy, and d) density.

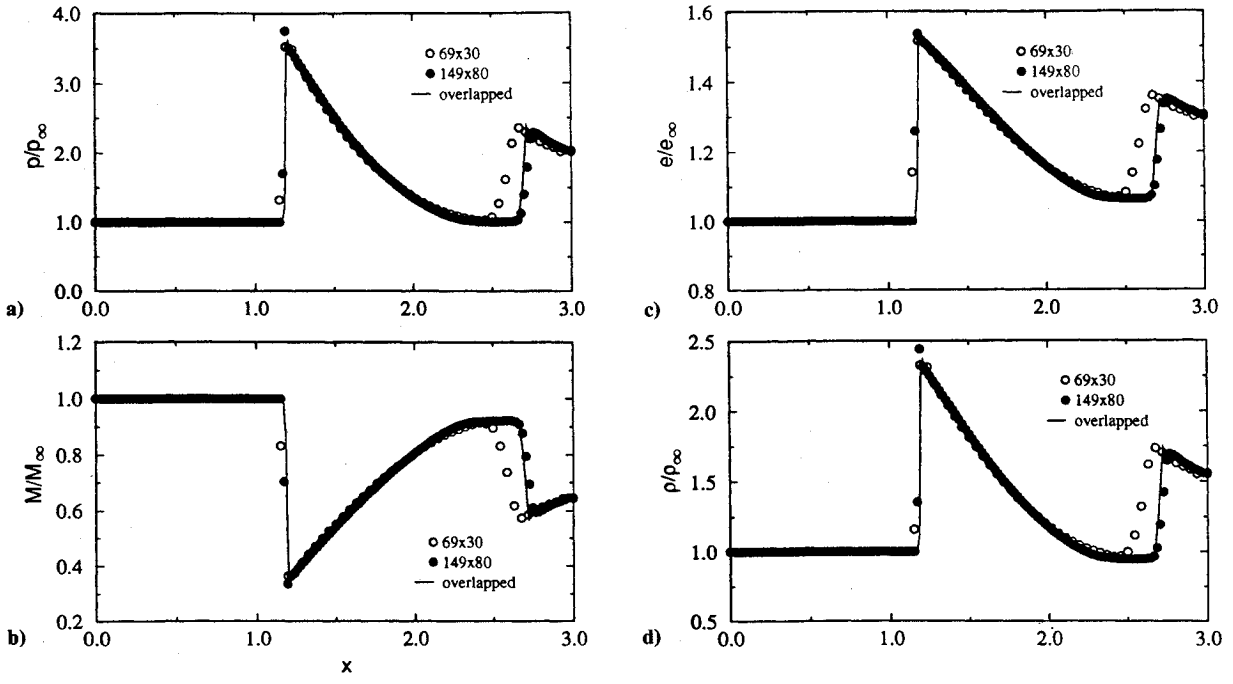

Fig. 11 Variable profiles along the upper solid wall: a) pressure, b) Mach number, c) internal energy, and d) density.

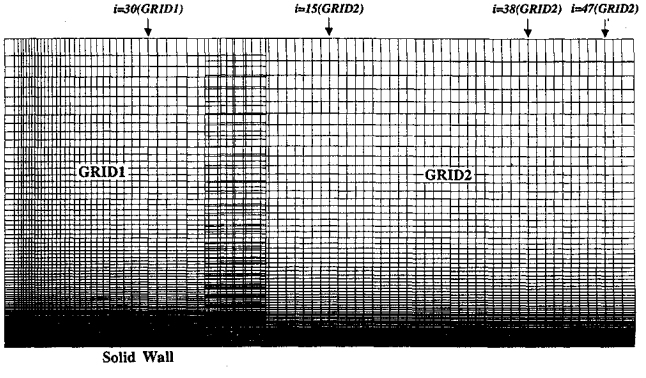

Fig. 12 Composite grid system for laminar flat-plate problem; GRID1 (40 × 100) and GRID2 (50 × 80).

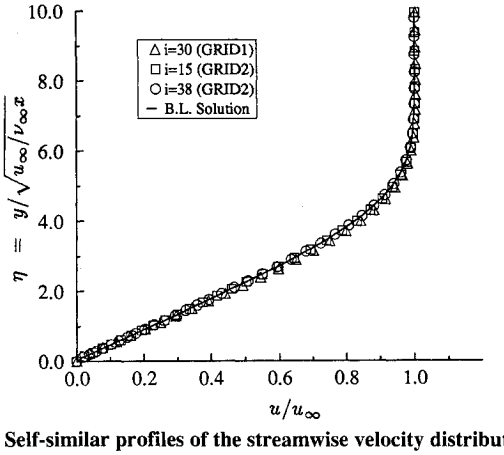

Fig. 13 Self-similar profiles of the streamwise velocity distribution at various downstream locations, $M_\infty = 2$.

the flow solutions can be enhanced after the adaptation. Furthermore, the grid orthogonality can be maintained in each grid and the convergence history will not suffer because of grid skewedness. For the test cases shown in this paper, the shock wave is the obvious feature for applying the adaptation procedure. However, in more complex flows, several adaptation criteria may be needed. Determinations in choosing various adaptive criteria, such as the density, pressure, etc., really rely on the users' knowledge. An automatic adaptive grid system is beyond the scope of the present study and will not be discussed herein.

IV. Test Problems and Result Discussions

The present grid adaptation method has been implemented for inviscid shock reflection, 15-deg ramp channel flow, laminar flat-plate, and shock wave/boundary layer interaction problems. The numerical results presented herein show the flexibility of the present method and the accuracy attainable by solution-based enhancement.

Case 1: Inviscid Shock Reflection

We consider a regular reflection of an oblique shock wave from a solid surface. The inflow conditions are fully specified with freestream values and the conditions at the top boundary are set to satisfy the shock-jump relations with a specified shock angle. The variables at the outflow boundary are extrapolated linearly. At the solid wall, the slip condition is applied by setting the normal velocity component and the gradient of other variables to zero.

The first case has an incoming Mach number of 2.9 and a shock angle of 29 deg. The computational domain contains four independent grid meshes. A base grid of size 59 × 20 is equally divided in a domain $0.0 \le x \le 4.0$, and $0.0 \le y \le 1.0$. Additional adapted grids are generated separately to align with the shock location based on a prescribed flow solution. In all cases, it is sufficient that the grid meshes are generated using an algebraic method which uses the edge point information to interpolate grid point values on the surface interior. Figure 3 illustrates the complete composite grid system. As denoted in the figure, GRID1 (59 × 20) represents the background coarse grid; GRID2 (29 × 50) and GRID3 (29 × 50) overset on top of the incoming oblique shock and on the outgoing reflection shock, respectively. The last grid, GRID4 (29 × 20), resolves the intersection region where the oblique shock impinges against the solid surface.

PEGSUS then composes each grid mesh together and provides the necessary interpolation data before proceeding to the flow solver. As displayed in Fig. 4, the base grids are excluded within the shock region. It is proposed that the shock structure will be resolved by the adapted overlapping grids. The pressure contours for the shock reflection are illustrated in Figs. 5a and 5b. It is shown that the shock wave structures are strongly enhanced (Fig. 5b).

Figures 6a–6c plot the comparisons of the pressure, density, and internal energy distributions between numerical calculation and the exact solution along $y = 0$. Note that the numerical results by the present method predict a sharp transition through the shock waves.

Case 2: Two-Dimensional Channel with a 15-deg Ramp

In this case, the steady-state flow is computed for a two-dimensional channel with a 15-deg ramp. The freestream Mach number is $M_\infty = 1.8$. There is an attached shock at the compression ramp corner which reflects from the top wall forming a Mach stem. The Mach number is chosen so that the extent of the Mach stem is about 20% of the channel height. The shock wave continues to reflect from the bottom and top walls, before exiting the channel. The ramp-shoulder expansion fan acts to weaken the first reflected shock. It is noted that a slip line emanates from the triple point at the Mach stem.

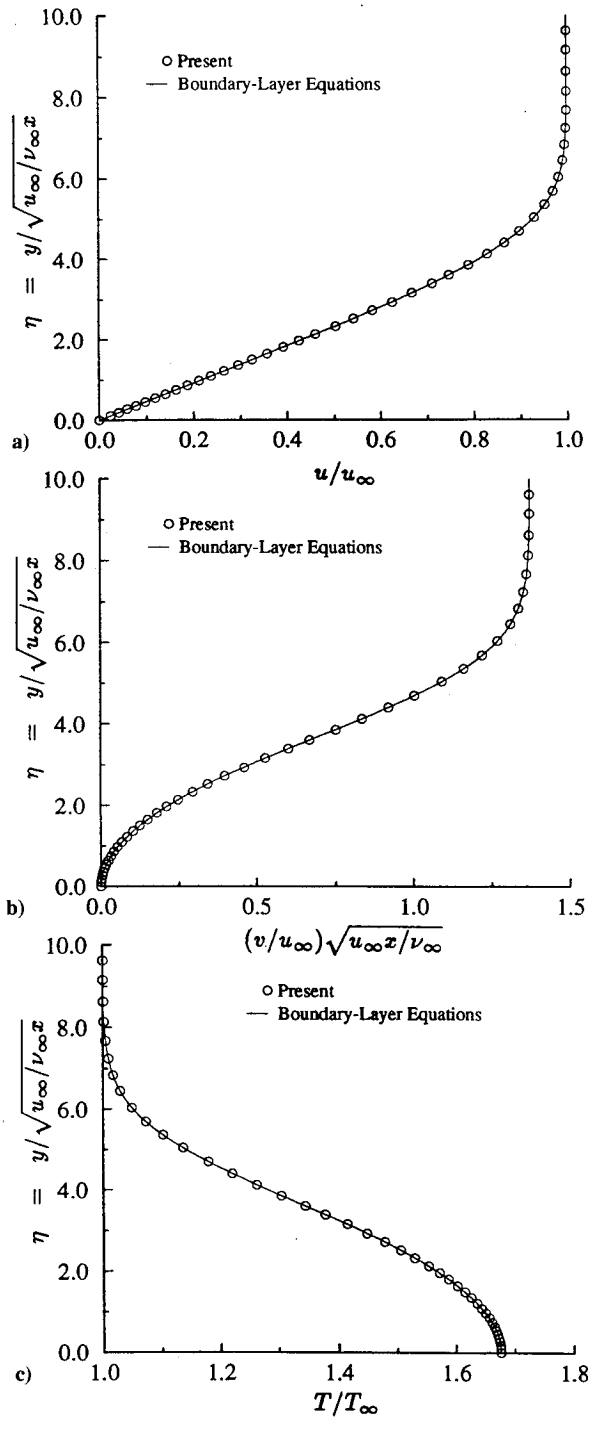

Fig. 14 Comparisons of velocity and temperature distributions at a downstream location: a) streamwise velocity, b) normal velocity, and c) temperature.

Numerical studies are performed based on three different types of grid system. The calculation is first carried out on a single uniform grid of size 69×30 for a domain ($0 \le x \le 3$ and $0 \le y \le 1$), as shown in Fig. 7a. Figures 7b and 7c plot the converged results of the flowfield in the form of pressure and Mach contours, respectively. The slip line emanating from the triple point is hardly observed, as shown in Fig. 7c. Note that the shock structures are not well resolved, suggesting that solution improvement is needed there.

By scanning the maximum pressure gradient points from the base grid solution, we adapt four additional meshes which are clustered and aligned with the shock waves. Figure 8a shows the connections of the composite grid system. The blanked regions indicating the hole locations on the base grid are displayed in Fig. 8b. In Figs. 8c and 8d both pressure and Mach contours give an overall qualitative picture of the flow, demonstrating a sharp resolution of the ramp shock, Mach stem, and the subsequent shocks. It is worth noting the clear slip line emanating from the triple point. In view of those contour plots, the ramp shock is clearly captured and the shock angle is about 51 deg. In addition, the subsequent shocks are also well-resolved.

To validate the preceding adapted solutions, numerical results are further obtained using a single fine mesh (149×80), as shown in Fig. 9a. Illustrated in Figs. 9b and 9c are the computed pressure and Mach contours, respectively. The detailed quantitative profiles along the lower and upper solid boundaries are compared among the present results and various single mesh solutions, as displayed in Figs. 10a–10d and 11a–11d. It is evident that the solution-adaptive overlapping meshes yield an accurate prediction for the ramp shock and subsequent shock locations along the lower surface in Figs. 10a–10d. No attempt has been made to adapt the ramp-shoulder expansion fan, so that the fan is slightly smeared due to the coarse grid structure. For the upper surface, Figs. 11a–11d show that the shock locations are also accurately predicted when the present method is applied. Also observed in the coarse grid solution, an early reflecting shock position is predicted. In general, we show that the coarse grid system has difficulty in predicting the correct locations for the oblique shock, Mach stem, and the subsequent shock waves. However, by using the overlapping adaptive meshes, we are capable of accurately capturing the shock structures and other salient features.

Case 3: Flat-Plate Boundary Layer Flow

A compressible, laminar flat-plate flow problem is computed to validate the implementation of chimera overset meshes for viscous flow. Figure 12 illustrates the composite grid system used in the computational domain. It contains two independent grid meshes with an overlapping region being used to connect the grid boundaries. The spacing of GRID1 (40×100) is constructed using a hyperbolic-tangent stretching function in the streamwise direction in the vicinity of the leading edge, followed by increasing cell spacing downstream. The second grid system, GRID2 (50×80), extends downstream using an equal-spacing distribution in the streamwise direction. A hyperbolic-tangent stretching function is applied to stretch the grid in the normal direction in both meshes with the first grid spacing $\Delta y_1 = 0.0015$. Note that the grid lines at the interface region are misaligned in an arbitrary orientation.

Boundary conditions include a Mach 2 freestream inflow, exit outflow extrapolation, and outflow extrapolation at the top boundary to avoid artificially constraining the normal velocity component. An inviscid wall is assumed forward of the plate leading edge. Laminar flow upstream of the leading edge starts to develop a boundary layer at the leading edge. A no-slip condition is applied on the adiabatic flat plate.

To validate our numerical results, comparisons are made between the present numerical results and those obtained by solving the boundary-layer equations.[19] The numerical solutions of the present method, as shown in Fig. 13, illustrate self-similar profiles of the streamwise velocity distributions at various downstream locations ($i = 30$ of GRID1, $i = 15$ and 38 of GRID2). Note that

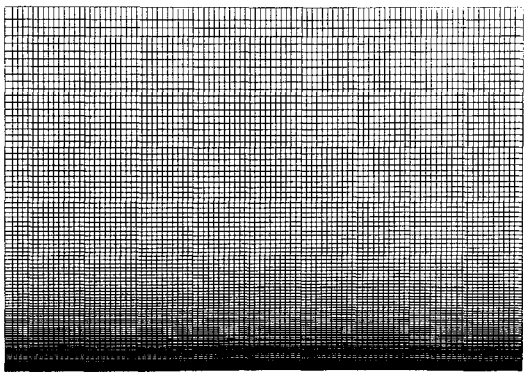

Fig. 15 Single fine grid system for the shock wave/boundary layer interaction (100 × 120).

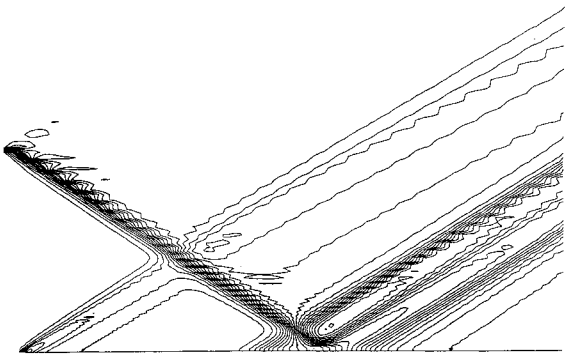

Fig. 16 Pressure contours for shock wave/boundary layer interaction problem with $M_\infty = 2.0$, $Re_\infty = 2.96 \times 10^5$, and shock angle = 32.585 deg ($p_{min} = 0.7$, $p_{max} = 1.1$, $\Delta p = 0.01$).

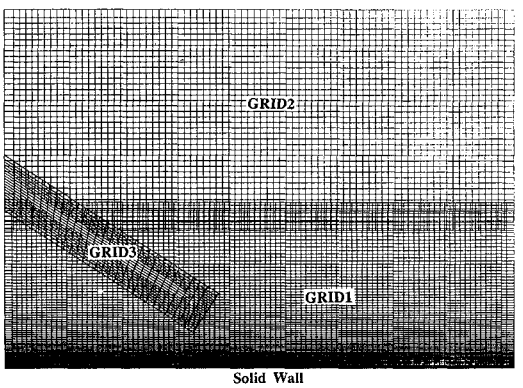

Fig. 17 Composite grid system for shock wave/boundary layer interaction problem; GRID1 (100 × 80), GRID2 (80 × 40), and GRID3 (30 × 20).

the profiles are plotted against a transformed coordinate $\eta = y\sqrt{u_\infty / \nu_\infty x}$. This mainly shows that the fluid fluxes are accurately transferred through the interfaces of grid boundaries. It is also found that such similarity extends to the normal velocity distributions and to the temperature fields. Figure 14a compares the streamwise velocity component between the present numerical result and the boundary-layer solution at a downstream location ($i = 47$ of GRID2) behind the grid interfaces. The normal velocity distributions and the temperature profiles are also compared in Figs. 14b and 14c, respectively. It is evident that the present method yields very good agreement with the boundary-layer solution, indicating that the accuracy of the numerical results using overlapping meshes is well preserved.

Case 4: Shock Wave/Boundary Layer Interaction

The current method is readily applied to the shock wave/boundary layer interaction problem. The experiment by Hakkinnen et al.[20] at $M_\infty = 2.0$, $Re_\infty = 2.96 \times 10^5$ and shock angle = 32.585 deg was chosen for calculation using the adapted overlapping grids. It is observed that the flow at the leading-edge shock wave induced by the start of the boundary layer becomes noticeably weaker after intersecting with an impinging oblique shock wave. The oblique shock is sufficiently strong to induce a sizable separation, which in turn causes the formation of the separation shock as the mainstream encounters a change of effective body. An expansion fan is created as the streamline changes slope, roughly at the pressure plateau. Finally the reattachment shock wave is developed corresponding to further rise of the pressure.

A single fine mesh using 100 × 120 in the streamwise and normal directions, respectively, is first chosen to simulate the Mach 2 flow. As displayed in Fig. 15, grid spacing in the normal direction is stretched near the solid boundary which allows a better resolution of the boundary layer. The resulting pressure contours are plotted in Fig. 16. Based on a coarse grid (50 × 60) solution, enhancement of the flow solution is also performed using overlap-

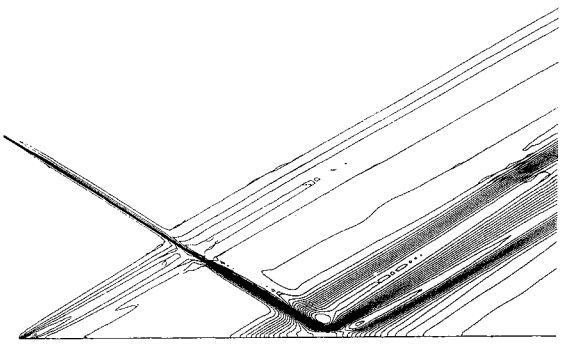

Fig. 18 Pressure contours for shock wave/boundary layer interaction with composite adaptive meshes ($M_\infty = 2.0$, $Re_\infty = 2.96 \times 10^5$, shock angle = 32.585 deg, $p_{min} = 0.7$, $p_{max} = 1.1$, $\Delta p = 0.01$).

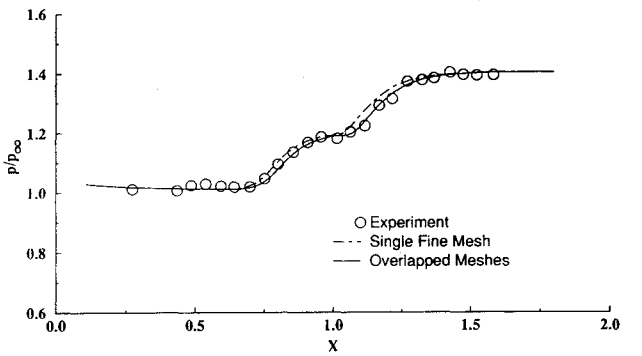

Fig. 19 Comparison of surface pressure ratio for shock wave/boundary layer interaction ($M_\infty = 2.0$, $Re_\infty = 2.96 \times 10^5$).

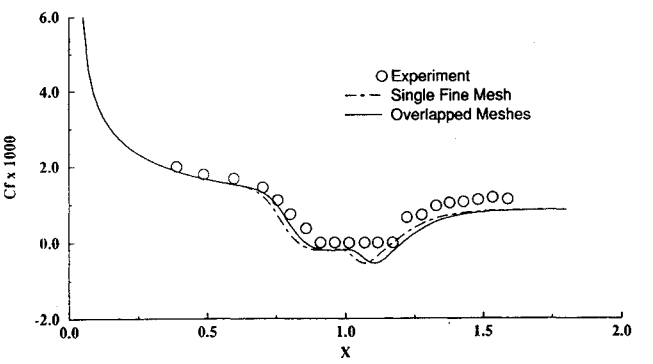

Fig. 20 Comparison of skin friction coefficient for shock wave/boundary layer interaction ($M_\infty = 2.0$, $Re_\infty = 2.96 \times 10^5$).

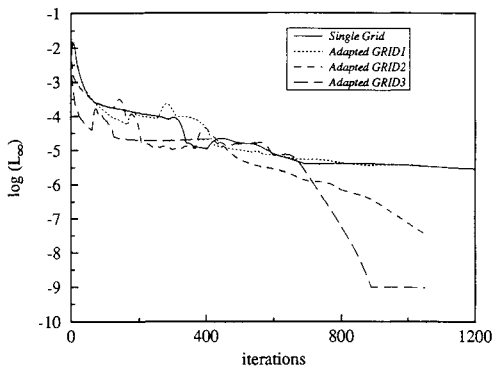

Fig. 21 Convergence history for shock wave/boundary layer interaction.

ping adaptive meshes. Figure 17 illustrates the solution-adaptive grid system which contains a total of 11,800 grid points in three independent meshes: GRID1 (100×80) resolves the boundary layer region; GRID2 (80×40) covers the flowfield beyond the boundary layer; and GRID3 (30×20) catches the incoming oblique shock wave. The number of overall grid points for the adaptive grid system is slightly less than that for the single-fine-mesh system. It is observed that the present method yields a significant improvement to the flowfield and, in particular, to the shock structures, as shown in Fig. 18. We further compare the pressure ratio and skin friction along the flat plate with those obtained by Hakkinnen et al.[20] While many other calculations have been reported, the reattachment point in general is much harder to predict accurately than the separation point. Figure 19 displays a very good agreement of the enhanced solution with the experimental data in the surface pressure ratio at both the separation and reattachment points. However, the skin friction in Fig. 20 shows a slight discrepancy in the separation region.

Figure 21 illustrates the convergence histories for the single-fine-mesh solution as well as for the overset adaptive-mesh solution. It is observed that the solutions for both grid systems start to approach steady-state conditions at around 900 iterations. The maximum residuals were found to occur near the shock wave/boundary layer interaction region in the boundary layer.

V. Concluding Remarks

We have presented a solution-adaptive enhancement method using chimera composite overlapping meshes and have shown its capability for crisply capturing high-gradient regions. Applications to various shock reflection and shock wave/boundary layer interaction problems were tested. The successful implementation of the chimera overset grid in combination with a Navier-Stokes solver serves as a useful tool that enhances the accuracy of salient features of the flowfield, such as shock and reflection waves. Unlike other grid adaptation methods, the present methodology would not create high-aspect-ratio or highly skewed cells in the grid system so that a reduced convergence rate is avoided. The strategy for chimera overset grids also provides a great flexibility in grid generation for complex configurations.

Acknowledgments

This research was in part supported by the NASA Lewis Research Center under Grant No. NCC3-168 through the University of Colorado. The first author would like to thank Ing-Tsau Chiu for his helpful discussions.

References

[1]Benek, J. A., Buning, P. G., and Steger, J. L., "A 3-D Chimera Grid Embedding Technique," AIAA Paper 85-1523, July 1985.

[2]Gnoffo, P. A., "A Vectorized, Finite Volume, Adaptive Grid Algorithm for Navier-Stokes," *Numerical Grid Generation*, edited by J. F. Thompson, North-Holland, New York, 1982, pp. 819–836.

[3]Brackbill, J. U., "Coordinate System Control: Adaptive Meshes," *Numerical Grid Generation*, edited by J. F. Thompson, North-Holland, New York, 1982, pp. 277–294.

[4]Saltzman, J., and Brackbill, J. U., "Applications and Generalizations of Variational Methods for Generating Adaptive Systems," *Numerical Grid Generation*, edited by J. F. Thompson, North-Holland, New York, 1982, pp. 865–884.

[5]Berger, M. J., "Adaptive Mesh Refinement for Hyperbolic Partial Differential Equations," STAN-CS-82-924, Stanford Univ., Stanford, CA, Aug. 1982.

[6]Eiseman, P. R., "Adaptive Grid Generation by Mean Value Relaxation," *Advances in Grid Generation*, edited by K. N. Ghia and U. Ghia, American Society of Mechanical Engineers, ASME-FED-5, 1983, pp. 29–34; also *ASME Journal of Fluids Engineering*, Vol. 107, 1985, pp. 477–483.

[7]Eiseman, P. R., "Adaptive Grid Generation," *Computer Methods in Applied Mechanics and Engineering*, Vol. 64, North-Holland, New York, 1987, pp. 321–376.

[8]Nakahashi, K., and Diewert, G. S., "A Three-Dimensional Adaptive Grid Method," AIAA Paper 85-0486, Jan. 1985.

[9]Gonnett, W. C., Agarwal, R. K., and Schwartz, A. L., "An Adaptive Grid-Generation Scheme for Flowfield Calculations," AIAA Paper 87-0199, Jan. 1987.

[10]Gonnett, W. C., Agarwal, R. K., and Schwartz, A. L., "An Adaptive Grid-Algorithm for the Euler/Navier-Stokes Equations," AIAA Paper 88-0519, Jan. 1988.

[11]Lombard, C. K., and Venkatapathy, E., "Implicit Boundary Treatment for Joined and Disjoint Patched Mesh Systems," AIAA Paper 85-1503, July 1985.

[12]Venkatapathy, E., and Lombard, C. K., "Flow Structure Capturing on Overset Patch Meshes," AIAA Paper 85-1690, July 1985.

[13]Ekaterinaris, J. A., and Schiff, L. B., "Vortical Flows over Delta Wings and Numerical Prediction of Vortex Breakdown," AIAA Paper 90-0102, Jan. 1990.

[14]Suhs, N. E., and Tramel, R. W., "PEGSUS 4.0 User's Manual," Arnold Engineering Development Center, AEDC-TR-91-8, Arnold AFB, TN, Nov. 1991.

[15]Benek, J. A., Steger, J. L., Dougherty, F. C., and Buning, P. G., "Chimera: A Grid-Embedding Technique," Arnold Engineering Development Center, AEDC-TR-85-64, Arnold AFB, TN, April 1986.

[16]Liou, M. S., and Hsu, A. T., "A Time Accutate Finite Volume High Resolution Scheme for Three Dimensional Navier-Stokes Equations," AIAA Paper 89-1994-CP, June 1989.

[17]Liou, M. S., and Steffen, C. J., Jr., "A New Flux Splitting Scheme," NASA-TM-104404, May 1991.

[18]Liou, M. S., "On A New Class of Flux Splittings," *13th International Conference on Numerical Methods for Fluid Dynamics*, Rome, Italy, July 1992, pp. 115–119.

[19]Cebeci, T., and Smith, A. M. O., *Analysis of Turbulent Boundary Layers*, Academic Press, New York, 1974, pp. 327, 328.

[20]Hakkinen, R. J., Greber, I., Trilling, L. and Abarbanel, S. S., "The Interaction of an Oblique Shock Wave with a Laminar Boundary Layer," NASA Memo 2-18-59W, 1959.